International Journal of Nanoelectronics and Materials
Volume 14, No. 3, July 2021 [269-280]

Rapid Response Room Temperature Oxygen Sensor Based on Trivalent-Elements Doped TiO_2 Thin Film

Nor Damsyik Mohd Said[1,2], Mohd Zainizan Sahdan[1,*], Nafarizal Nayan[1], Anis Suhaili Bakri[2], Nur Amaliyana Raship[2], Hashim Saim[2], Kusnanto Mukti Wibowo[2], Feri Adriyanto[2]

[1]*Microelectronic and Nanotechnology—Shamsuddin Research Centre (MiNT-SRC), Universiti Tun Hussein Onn Malaysia, 86400 Parit Raja, Batu Pahat, Johor, Malaysia.*
[2]*Department of Information Technology & Communication, Politeknik Mersing, Jalan Nitar, 86800 Mersing, Johor*

Received 3 March 2021, Revised 13 May 2021, Accepted 9 June 2021

ABSTRACT

Trivalent metal-doped TiO_2 thin films have been extensively investigated in gas sensor applications. The trivalent metal dopants are Al, Y and Gd. The trilayer fabrication of a gas sensor consists of a thin film, sputtered TiO_2 and Au nanoparticles. The characteristics of the gas sensing properties are strongly correlated with the annealing temperature, film thickness, type of doping and deposition method. The subsequent properties are presented – the crystalline structure, grain size, roughness, strain, stress and defects. Thin films have been developed with concentrations of O_2 gas up to 10 sccm. A response time for O_2 gas in milliseconds was obtained at room temperature. Al doped TiO_2 thin film have a faster response time operating at room temperature compared with other thin films. Oxygen vacancy defects also contribute to the speed of the response time for a gas sensor.

Keywords: Titanium Dioxide, Nanomaterial, Spin Coating

1. INTRODUCTION

Some scientists have developed semiconductor-based nanostructures by their characterisation. Semiconductor-based nanostructures are very important to produce effective new nanomaterials at low cost. Nanomaterials can be used to produce oxygen gas sensors to determine when the levels of oxygen could be dangerous, either at under or over limitation. The development of atoms or molecules with arbitrary orientations is produced by a gas sensor. Nevertheless, gas sensors are commonly inadequate in terms of sensitivity and the stability is only appropriate for high temperatures applications [1]. Titanium dioxide (TiO_2) is one of the promising materials that could be operated as a gas sensor reliant on the alteration of its resistivity. In addition, it has good sensitivity when in contact with oxygen (O_2) gas [1], good response [2], chemical constancy [3] and a reversible process [4]. The detecting properties of TiO_2 thin film is based on the annealing temperature, thickness of the film, deposition technique and the subsequent properties such as the crystalline structure. Additionally, the trivalent dopants such as Al [5], Y [6] and Gd [7] can be combined with the TiO_2 thin film so that the response time improves. A trivalent dopant has three ionic states. Therefore, a trivalent dopant can contribute defects when the mobility of the hole carrier is high and the electrons of Ti can move easily from Ti^{4+} to Ti^{3+}. This thin film oxidises the gas because of its n-type material. A trivalent dopant generates oxygen vacancies in the TiO_2 lattice. Oxygen vacancies are the defect state to enhance

*Corresponding author: *zainizan@uthm.edu.my*

the performance of a gas sensor. Further, the importance of dopant accumulation in TiO_2 is based on its resistivity, conductivity, sensing properties and having a high surface ratio [8].

Rajnish K. Sharma *et al.* investigated TiO_2 doped with chromium using a sol-gel technique. A short response time (5 s) was measured at 700 °C for a 0.40 wt% Cr doped sensor as compared to an undoped sensor, which also indicated a sensitivity of 13 times higher at 800 °C. The implementation of thin films shows that the porosity of the thin film decreases as the Cr concentration increases, although its performance was achieved at a high pressure of oxygen gas. The performance of the thin films can be improved at a low pressure of oxygen gas as this influences the sensitivity. Linhui Gan *et al.* investigated Nb doped TiO_2thin films prepared by the facile sol-gel method. After optimisation, 6 % Nb doped TiO_2 also showed the most rapid response time of 1.1 s at 700 °C annealing temperature. Nevertheless, it was still activated at a high temperature.

This study aims to determine the sensor response of undoped TiO_2 films and doped thin films to O_2 gas to be analysed based on O_2 concentration at room temperature by means of measuring their voltage. In previous research, TiO_2 thin film have been synthesised with pure TiO_2, Al doping, Y doping and Gd doping. The phase stability, surface morphology and topology of the TiO_2 thin film is also to be characterised converging on oxygen gas sensing.

2. EXPERIMENT

2.1 *Fabrication of the electrodes*

A thermal evaporator machine was used to fabricate the 160 nm thick Au electrodes deposited on thin films. The Au electrode array pattern was designed using AutoCAD software. Figure 1 shows the fabrication of the trilayer and Au electrodes on a glass substrate.

2.2 *Preparation of the trilayer*

The thin film consists of three layers is prepared as follows:

(i) Nanogold layer

The Au nanoparticles were obtained by immersion for 3 hours by applying the seeding and growing process as shown in Figure 1(a)

(ii) Sputtered TiO_2 layer

Figure 1(b) shows the deposition process for the sputtered TiO_2 layer as applied in this work [2]. The TiO_2 layer had the following specification for the RF sputtering:

i. Power: 200 W
ii. Deposition time: 15 minutes
iii. Temperature: 300 °C

(iii) TiO_2 sol was firstly prepared based on the sol-gel method. Titanium (IV) butoxide ($Ti(OC_4H_9)_4$ (Sigma Aldrich, 97 %) was used as a precursor, ethanol as a solvent (C_2H_5OH), deionised water as a function of adding the oxygen (O), acids and triton X-100 ($C_{14}H_{22}O(C_2H_4O)_n$) (Sigma Aldrich). Moreover, glacial acetic acid (CH_3CO_2H) and hydrochloric acid (HCl) were added. Before that, the sols were stirred for 30 minutes at 45 °C. Then, an ageing process was utilised for 3 hours. Dopant precursors such as aluminium nitrate nanohydrate ($Al(NO_3)_3 \cdot 9H_2O$)(SigmaAldrich, ≥98 %), yttrium(III) nitrate hexahydrate ($N_3O_9Y.6H2O$) (Sigma Aldrich, 99.8 %) and gadolinium(III)

acetate hydrate ($C_6H_9GdO_6.xH_2O$) (Sigma Aldrich, 99. 9 %) were added and the doping process conducted one by one. Then, the sol thus obtained was spin-coated on the glass substrate. The speed of the spin coater was 3000 rpm for 30 s to combine five layers of uniform films. Subsequently, TiO_2 solution was released for 10 times onto the glass substrate. Then, the formed layers were preheated at 100 °C for 5 min. The thin films were then annealed at 500 °C for one hour as shown in Figure 1(c) [4].

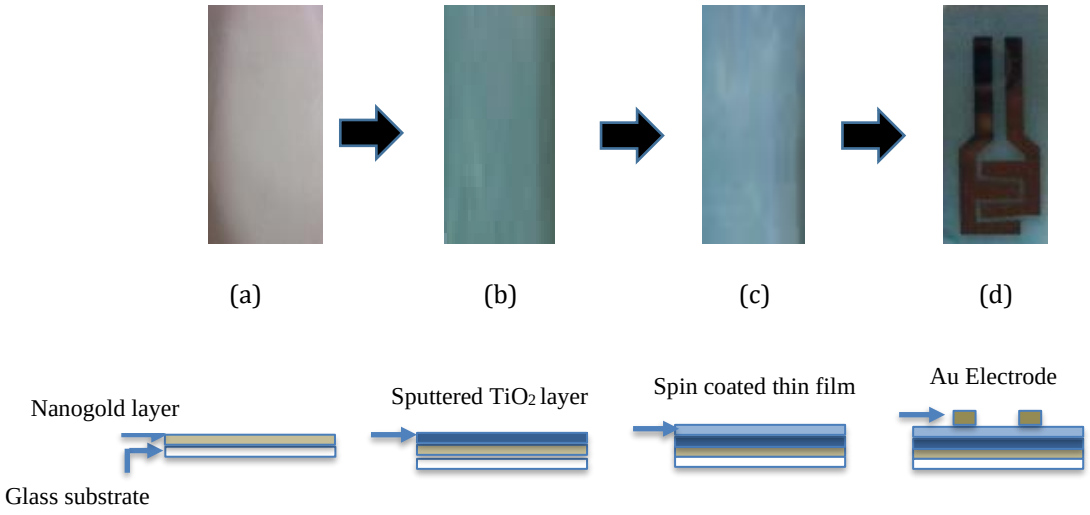

Figure 1: Sample deposition on glass substrate: (a) nanogold layer, (b) sputtered TiO_2 layer, (c) spin coated thin film (pure TiO_2/ doped TiO_2), (d) Au electrodes

2.3. Characterisation of the TiO_2 thin films

To identify the crystalline phases of the unknown nanomaterial, PAnalytical Smartpowder X-ray diffractometer (XRD) is used. The measurement was obtained at 2θ by Cu Kα radiation. The thickness of the TiO_2 film was identified by cross section with a Field Emission Scanning Electron Microscope (FESEM), Jeol: JSM-7600F with an accelerating voltage of 15 kV. The surface topography of the films was captured and examined by an Atomic Force Microscope (AFM), XE-100 Park system at room temperature. This characterisation method promised a non-destructive testing.

2.4. Measurement technique

A computer-measured experimental setup was operated for the gas-response measurements and the oxygen gas sensor circuit as illustrated in Figure 2(a) and Figure 2(b), respectively. All measurements were undertaken in a sealed chamber with a capacity of $2.01x10^{-3}$ m^3. Before measurements were taken, purging of the chamber using Argon gas was conducted for 5 minutes to eliminate any contamination. The circuit was tested in the chamber. Gas flow to the chamber was organised by a Mass Flow Meter and controller by a Sierra StarTrak 50, with O_2 at 10 sccm (standard cubic centimetres per minute), respectively. A rotary pump was used to carry the oxygen gas. DC power was supplied by a Function Generator. This setup was used to measure the voltage V of the TiO_2 thin films up to 2.5 V for various O_2 concentrations and operating at room temperature. The performance of the thin film gas sensor was estimated by measuring the relative change in voltage with and without exposure to oxygen gas. The voltage output (Vg) of the gas sensor was displayed on an Oscilloscope.

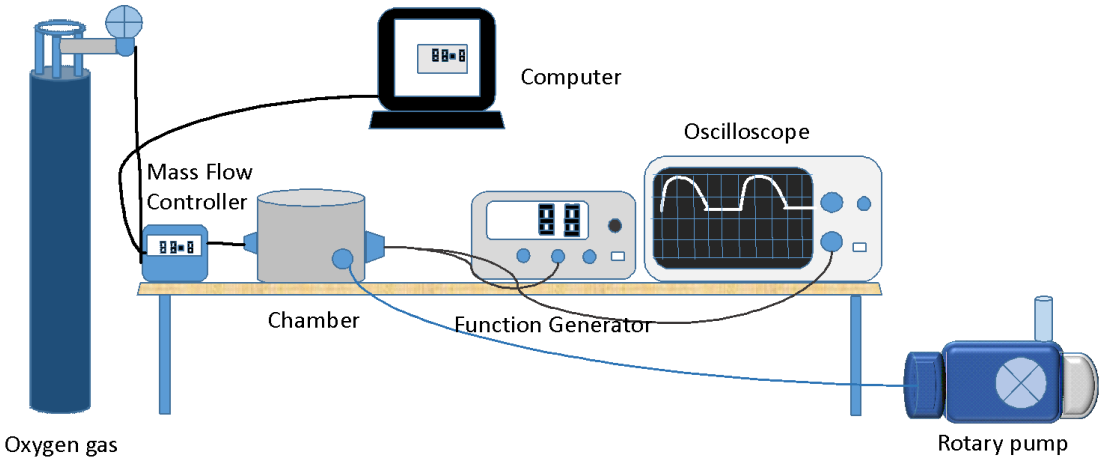

(a)

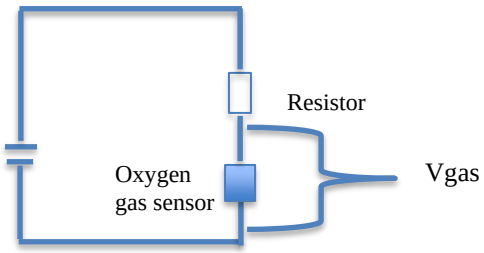

(b)

Figure 2: (a) A computer-measured experimental setup
(b) Oxygen gas sensor circuit

3. RESULTS AND DISCUSSION

The XRD experimental data indicated the standard TiO_2 patterns of anatase. The XRD measurements verified that the TiO_2 was mainly in the anatase (A) phase as shown in Figure 3. Moreover, the strong bulk diffraction lines were for A (101) yet the dominant peaks revealed that the films after annealing were orientated with respect to the glass substrate. The thin film consisted of a polycrystalline structure because of the contribution of the sputtered TiO_2 layer as a second layer when the thin films were annealed at 500 °C. For the undoped TiO_2, the XRD peaks were (25.3599), (38.1899), (44.4592), (48.1147), (54.005), (55.1836) corresponding to (101), (004), (221), (200), (105) and (211). All the peaks were anatase phase except one peak that was brookite phase at (44.4592). This effect arose from the sputtered TiO_2 layer when annealed for the second time. For the Al doped TiO_2 XRD the peaks were (25.3781), (38.1872), (48.1264), (54.0587) and (55.1894) corresponding to (101), (004), (200), (105) and (211). There was no brookite phase peak. For the Y doped TiO_2, the XRD peaks were (25.3407), (38.2816), (44.4647), (48.1021), (54.0108), (55.1073) corresponding to (101), (004), (221), (200), (105) and (211). All the peaks were anatase except for one peak that was brookite phase at (44.4647). This effect arose from the sputtered TiO_2 layer when annealed for the second time. Other than that, the second peak was apparently the highest intensity compared to the other thin films. However, the

orientation of the crystallite did not influence the performance of the thin film due to only the z axis being involved [3,4].

For the Gd doped TiO_2, the XRD peaks were (25.3046) and (38.2132) corresponding to (101) and (004). All the peaks were anatase phase and a slight intensity of two peaks could be observed. It also showed that the smaller nanoparticles for the Gd doped TiO_2 influenced the intensity of the thin film. The crystal size of the Al doped TiO_2 had a smaller average size compared to the undoped TiO_2. The situation could be explained by the quantum size effect shown in Table 1. This also correlated to the optimisation of the Al substitution on the Ti sites. It is well known that doping of foreign atoms in TiO_2 tends to change the lattice structure. The dopants used here were Al, Y and Gd, which have smaller, larger and even larger atomic radii than Ti, respectively. Moreover, no significant changes in the lattice parameters were observed for the Al doping concentration. On the contrary, the ionic radius of T^{4+} was 0.074 nm, which was smaller compared with Y^{3+} at 0.088 nm. Therefore, when Y^{3+} was inserted into the lattice of TiO_2, the diffraction intensity tended to be lower and the diffraction peak observed was broader which resulted in lower crystallinity. The XRD investigations confirmed that deposited Gd doped TiO_2 thin film normally influenced the development process, which had a prominent influence on their microstructure [4].

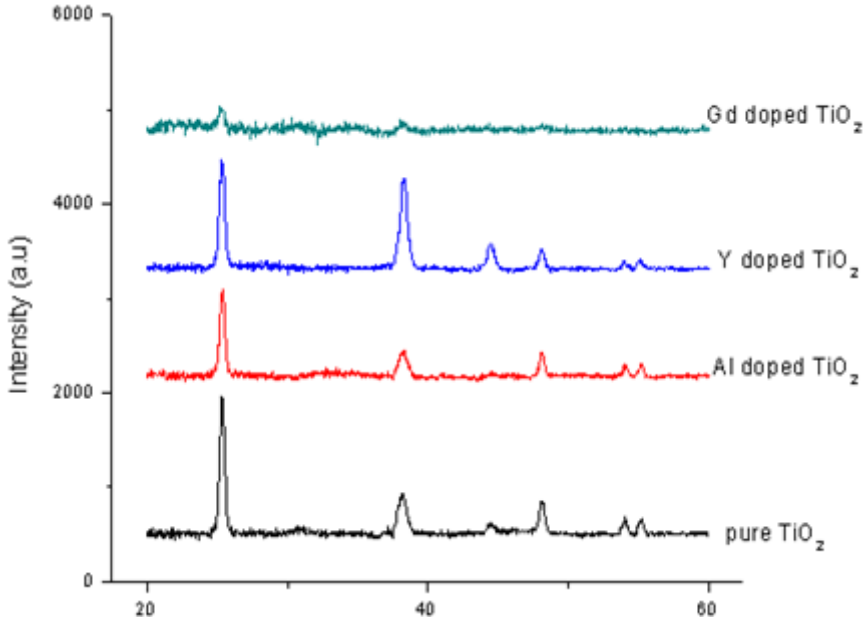

Figure 3: XRD peak for a gas sensor to pure TiO_2 and doped TiO_2 thin films

The crystal size (D) formula can be shortened as follows:

$$D = \frac{0.9\lambda}{\beta \cos\theta} \tag{1}$$

The fractional change in the length is expressed as strain (ε) and the dislocation density (δ) is described as the measurement of the length of dislocation lines in a unit volume of crystalline material, and applied using the simple approach of Freund and Suresh [5]:

$$\varepsilon = \frac{|c - c_o|}{c_o} \times 100\% \tag{2}$$

$$\delta = \frac{1}{D^2} \tag{3}$$

The stress (σ) formula of the equipped thin films is computed using the following [5]:

$$\sigma = \frac{2c^2 13 - c_{33}(c_{11} + c_{12})}{2c_{13}} x \frac{c - c_O}{c_O} \quad (4)$$

where, c_{11}=208.8 GPa, c_{33}=213.8 GPa, c_{12}=119.7 GPa and c_{13}=104.2 GPa [5]. The crystal sizes of 40.378 nm, 26.345 nm, 33.665 nm and 26.341 nm corresponding to pure TiO_2 for the trivalent dopant namely Al, Gd and Y, respectively. The dominant (101) peaks were as-synthesised between the thin films [6]. Further, the full width at half maximum (FWHM) was wider with a smaller crystallite size depending on the doping concentration. The smaller crystallite size caused an increase of the dislocation of the thin films. In linear defects, groups of atoms would be in unbalanced positions and the atoms tend to be out of position in the crystal structure [7]. For all thin films, the dislocation of a thin film increases and the stress produces tensile thin films due to the positive sign. Then, a and c tend to increase as shown in Table 1.

Dislocations may also be generated and moved when a stress was applied. Dislocation controls the strength and ductility of metals. Dislocation for the Al doped TiO_2 and Gd doped TiO_2 thin films created a large change. However, there tended to be only little strain in Gd doped TiO_2 thin films so the stress showed only a little change. This means that a small amount of strain could occur when a Gd dopant atom substitutes a Ti atom in a semiconductor lattice. The volume of a thin film could also alter when the ion radius of the Gd dopant and the Ti elements have different sizes. In addition, the strain for Y doped TiO_2 thin film may increase by a high amount compared to other thin films because that strain energy may control the Y dopant solubility in the TiO_2 semiconductor, especially if the size difference between the Y dopant and the Ti elements was large. When a material was loaded with a force, strain produced stress, which then causes the material to deform. Strain and stress in a semiconductor may also contribute to changes in the defect states. Stress refers to the pressure or tension used on a material object. The existence of strain within atoms in a lattice could cause change in the physical properties and the device obtained from such materials could have increased performance of the thin film [8].

Table 1: Peak properties of gas sensors to pure TiO_2 and doped TiO_2 thin films

Pure and doped TiO_2 Con.	Position 2 theta(°)	Intensity (cts)	FWHM, deg	Calculated crystallite size, D (nm)	Dislocation ($x10^{15}$)	Strain	Stress GPa	Lattice constant	
								a	C
Pure	25.3599	330.34	0.2362	34.47	0.841	0.147	0.343	3.7760	9.4860
Al	25.3781	320.73	0.3542	22.99	1.892	0.147	0.343	3.7760	9.4860
Y	25.3407	384.96	0.252	32.31	0.957	0.189	0.441	3.7850	9.4820
Gd	25.3046	70.23	0.3542	22.99	1.892	0.0526	0.123	3.7860	9.4950

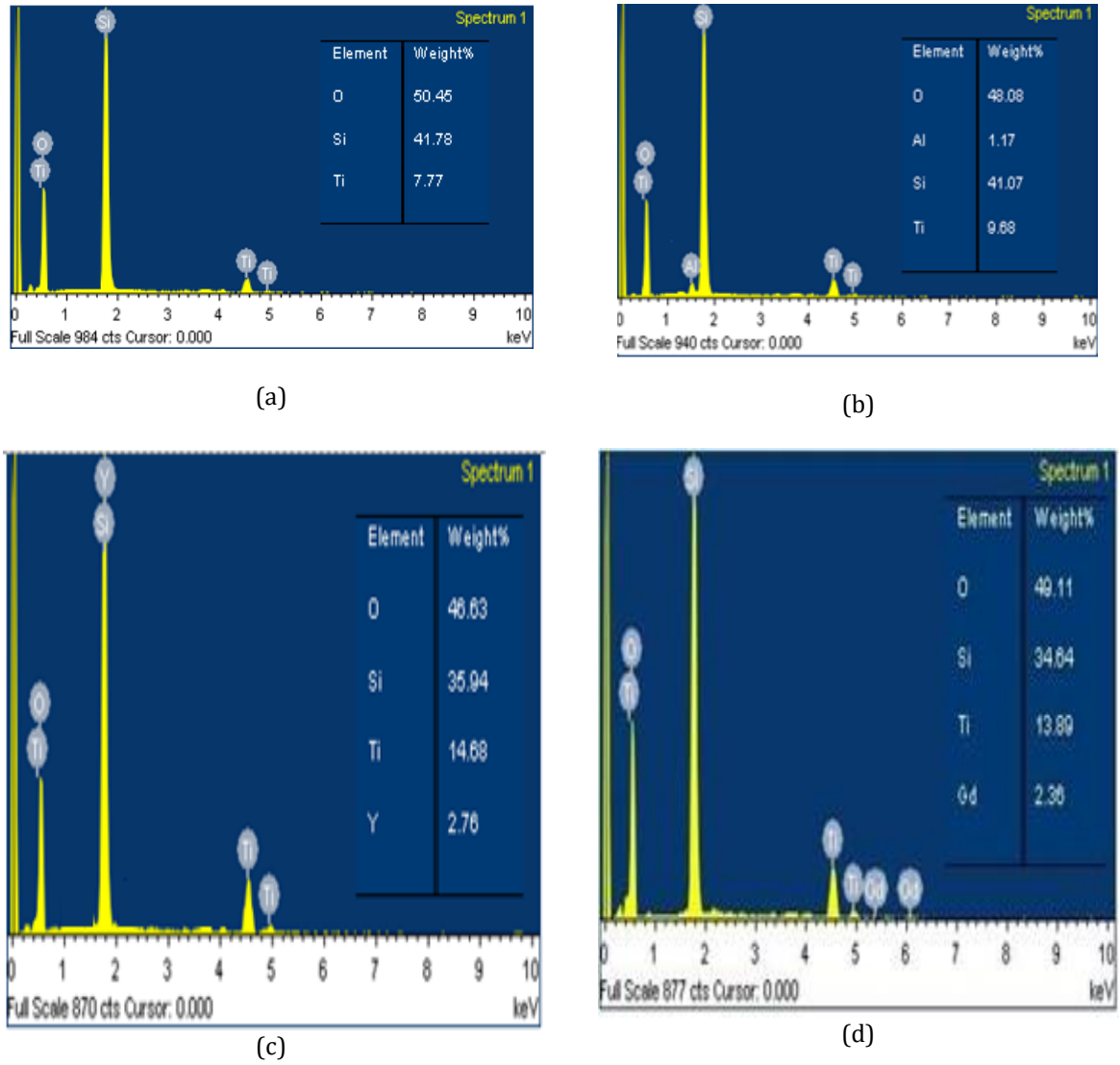

Figure 4: EDS peak for a gas sensor for: (a) pure TiO_2, (b) Al doped TiO_2, (c) Y doped TiO_2, (d) Gd doped TiO_2

Figure 4 shows the percentage of weight of Al doping concentration, Y doping concentration and Gd doping concentration corresponding to 3 wt. %, 4 wt. % and 4 wt. %, respectively. The spectrum elements for each thin film were revealed using energy-dispersive X-ray spectroscopy (EDS) and the spectrum indicated the existence of Titanium (Ti), Oxygen (O) and Silicon (Si) elements and trivalent dopants. High peaks of Si were found in all samples because of the silicon substrate. Therefore, this proves that trivalent metal-doped TiO2 has been formed as supported by the XRD data in Figure 3.

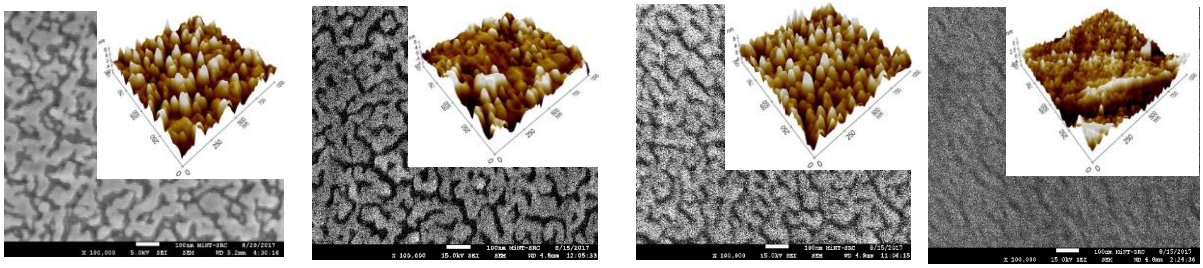

(a) (b) (c) (d)

Figure 5: Surface morphology and topography of a gas sensor to (a) pure TiO_2 (b) Al doped TiO_2 (c) Y doped TiO_2 (d) Gd doped TiO_2

Table 2: Grain size and roughness of oxygen gas sensors to pure TiO_2 and doped TiO_2 thin film

	Grain Size	Roughness
Pure TiO_2	48.125 nm	2.294 nm
Al doped TiO_2	55.095 nm	1.706 nm
Y doped TiO_2	50.778 nm	2.021 nm
Gd doped TiO_2	68.000 nm	0.747 nm

The effect of a faster response time could be due to the influences of the structural properties of the thin films in the figure, as the diffusion kinetics of the surface morphology did not have an effect. Figure 5 shows the surface morphology of the undoped TiO_2 and doped thin films. It was observed that the porosity of thin films could possibly provide advantages for gas sensor applications. Figure 5 also shows that the AFM surface topography of the doping concentration of the thin films indicated that the roughness of the doping concentration of the thin films was around 0.7 to 2.3 nm and annealed at 500 °C. This revealed that the roughness achieved the minima value, good homogeneity and smoothness of the TiO_2 particles on the surface. However, the thin film appeared to be non-uniform in the FESEM image. It may be noted that the morphology of the TiO_2 has a granular grain size.

The grain size was also about 48 to 68 nm as shown in Table 2. However, the higher amount of defects was due at least to the grain boundaries. Smaller grain sizes for thin films are encouraging as this improves the surface to volume ratio, the carrier concentration and makes collaboration easier with a higher number of gas molecules. The synthesis parameters and addition of suitable dopants with appropriate host materials played a main role in the sensitivity of the gas sensor. For undoped TiO_2 as shown in Figure 5(a), it was found that there was a smaller grain size and was one of the reasons that caused a faster response time. However, in this research, the faster response time of the doping concentration was the focus. After doping, the smaller crystallite size had an influence as well. It appeared that the films were uniform and pinholes were detected for each thin film and this showed that the morphology had a smaller grain size and was distributed homogeneously, which signified the crystalline nature of the film. The exception was for Gd doped TiO_2 thin film that appeared to be pinhole free. There was no evidence of cracking for each thin film [9]. It was also found that the Gd-doped TiO_2 layer displayed a smoothness of the microstructure (Figure 5(d)) compared to the undoped TiO_2 (Figure 5(a)), Al-doped TiO_2 (Figure 5b) and Y-doped TiO_2 (Figure 5()). Analogous to the AFM images, the grain size was clearly recognisable in the top view FESEM of TiO_2. It indicated that the lower roughness value showed that there was good homogeneity of the surface. The change in the grain shape was determined by analysing the XRD data as shown in Table 2.

At first, the voltage of the films were Vair ~ 0.79 V at room temperature. In Figure 6, the gas sensor response for each type of thin film is shown. The response time and the sensitivity of the gas sensor are shown in Table 3 and Table 4, respectively. Among the dopants, the Al doping concentration presented a delay of phase transformation from anatase to rutile by retaining the surface state of the TiO_2 nanoparticles and prevented grain growth [10]. The ionic radii of Ti^{4+} and Al^{3+} corresponded to 0.074 nm and 0.0675 nm, respectively. Al acted as a consistent cation position to create substitutional defects. The ionic radii of Y^{3+} and Gd^{3+} showed as interstitial defects owing to the larger ionic radius. Then, these substitutions could produce the oxygen vacancy defects required [11]. The sensitivity towards the target increased due to the dopant accumulation in the TiO_2. After optimisation, the Al doped TiO_2 gained a higher response because of the surface morphology and the characterisation of the crystal. By using the spillover effect, Au mixed with the semiconductor to catalyse gas sensing.

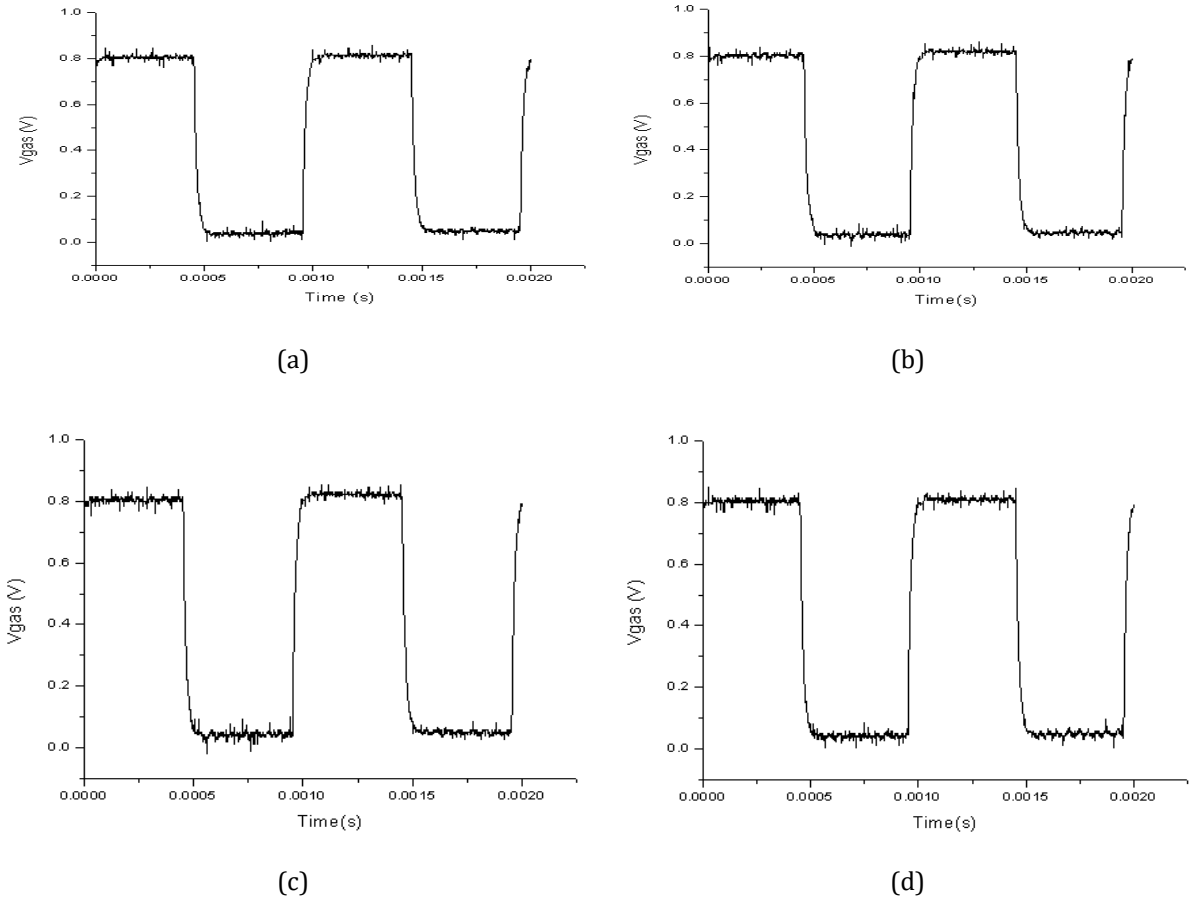

Figure 6: The sensor response of thin film: (a) pure TiO_2, (b) Al doped TiO_2, (c) Y doped TiO_2, (d) Gd doped TiO_2

Table 3: The response time of oxygen gas sensors corresponding to pure TiO_2 and doped TiO_2 thin films

Type of doping	Response time
pure TiO_2	29.098 ms
Al doped TiO_2	28.015 ms
Y doped TiO_2	30.400 ms
Gd doped TiO_2	29.752 ms

Table 4: The sensitivity of oxygen gas sensors corresponding to pure TiO_2 and doped TiO_2 thin films

Type of gas sensor	Vg	Va	Sensitivity (Vg-Va)/Va
pure TiO_2	0.156553	0.003789	40.32
Al doped TiO_2	0.156553	0.00256	60.15
Y doped TiO_2	0.140472	0.009796	13.34
Gd doped TiO_2	0.124392	0.003789	31.83

The highest sensitivity of the gas sensor was because of oxygen vacancy. Oxygen vacancies cause the surface conductivity to rise due to the adsorbed oxygen ions acting as surface acceptors, binding electrons and lessening the surface conductivity of the thin film [12]. The trivalent dopant increases the concentration of oxygen vacancies in the titania lattice portion [13].

A trivalent dopant generates oxygen vacancies in the TiO_2 lattice. Oxygen vacancies are the defect state to enhance the performance of a thin film. The higher the level of presence of oxygen vacancy defects could increase the conductivity of the thin film. Therefore, this could influence the response time and the recovery time of the thin film. [14] Additionally, the conductivity increased assuming that it would be under low oxygen partial pressure, due to the creation of ample oxygen vacancies [11].

The collaboration of O_2 with TiO_2 surfaces is important in the chemical sensing process. A fundamental reaction of oxygen adsorption is that it strongly influences the chemical features and charge carrier densities [15]. Other than that, O_2 adsorption and its interaction with the reduced anatase (101) surface, the oxygen vacancies and Ti interstitials have been revealed to inhabit the subsurface, while controlling the creation of a surface connecting dimer defects reconciled by the interaction of O_2 with a subsurface O vacancy. Likewise, the interaction of O_2 with a Ti interstitial produces transmission from the surface defect for the creation of a surface TiO_2 cluster. The superoxo (O_2-) states of the adsorbed molecules could be related with this experiment performed at room temperature that influences the width of the space charge region for each thin film [16].

4. Conclusion

Metal oxide films produced by sol-gel spin coating methods have been demonstrated at room temperature. The development of thin film must be investigated to explain the response to target oxygen gas. The factors of the sensing element affect the performance of the thin film namely the grain size and oxygen vacancy defects. By selecting dopants such as Al, Y and Gd, alongside the ionic radii, this gives the possibility of influencing the space charge region for better sensing.

Acknowledgement

The authors acknowledge the Fundamental Research Grant Scheme (FRGS) vot No. 1093 provided by the Ministry of Education Malaysia. The authors also acknowledge the technical support from Universiti Tun Hussein Onn Malaysia (UTHM).

References

[1] H. Wang, L. Chen, J. Wang, Q. Sun, and Y. Zhao, “A micro oxygen sensor based on a nano sol-

gel TiO_2 thin film," *Sensors (Switzerland)*, vol. 14, no. 9, pp. 16423–16433, 2014.

[2] S. H. Abdullah, M.Z.Sahdan,N. Nafarizal, H. Saim, A.S. Bakri, C.H. Rohaida, F.Adriyanto, and Y.Sari "Photoluminescence study of trap-state defect on TiO_2 thin films at different substrate temperature via RF magnetron sputtering," IOP Conf. Series: Journal of Physics: Conf. Series 995, 012067, 2018.

[3] A. Arunachalam, S. Dhanapandian, and C. Manoharan, "Effect of Sn doping on the structural, optical and electrical properties of TiO_2 films prepared by spray pyrolysis," *Phys. E Low-dimensional Syst. Nanostructures*, vol. 76, pp. 35–46, Feb. 2016.

[4] N. D. M. Said, M. Z. Sahdan,a N. Nafarizal, H. Saim, F. Adriyanto, A. S. Bakri a and M.Morsin, "Difference in structural and chemical properties of sol-gel spin coated Al doped TiO_2, Y doped TiO_2 and Gd doped TiO_2 based on trivalent dopants," *RSC Adv.*, vol. 8, no. 52, pp. 29686–29697, 2018..

[5] L. B. Freund and S. Suresh, *Thin Film Materials: Stress, Defect Formation and Surface Evolution*. Cambridge University Press, 2004.

[6] T. Xie *et al.*, "UV-assisted room-temperature chemiresistive NO_2 sensor based on TiO_2 thin fi lm," vol. 653, no. 2, pp. 255–259, 2015.

[7] B. Tryba, S. Jafari, M. Sillanpää, A. Nitta, B. Ohtani, and A. W. Morawski, "Applied Surface Science In fl uence of TiO_2 structure on its photocatalytic activity towards acetaldehyde decomposition," vol. 470, no. August 2018, pp. 376–385, 2019.

[8] X. Qu *et al.*, "Results in Physics Yttrium doped TiO_2 porous film photoanode for dye-sensitized solar cells with enhanced photovoltaic performance," *Results Phys.*, vol. 6, pp. 1051–1058, 2016.

[9] Y. Yang *et al.*, "Structure and crystal phase transition effect of Sn doping on anatase TiO_2 for dichloromethane decomposition," vol. 371, no. November 2018, pp. 156–164, 2019.

[10] H. A. R. A. Hussian, M. A. M. Hassan, and I. R. Agool, "Synthesis of titanium dioxide (TiO_2) nanofiber and nanotube using different chemical method," *Optik (Stuttg).*, vol. 127, no. 5, pp. 2996–2999, 2016.

[11] V. K. Ashith, G. K. Rao, R. Smitha, and S. N. Moger, "Study of micro-structural, optical and electrical properties of TiO_2 films obtained from micro-controller based SILAR method," *Ceram. Int.*, vol. 44, no. 15, pp. 17623–17629, 2018.

[12] Y. Gönüllü, G. César, M. Rodríguez, B. Saruhan, and M. Ürgen, "Sensors and Actuators B : Chemical Improvement of gas sensing performance of TiO_2 towards NO_2 by nano-tubular structuring," vol. 169, no. 2, pp. 151–160, 2012.

[13] V. G. Krishnan, P. Elango, V. Ganesan, and P. Sathish, "pH deeds on structural, optical, electrical and gas sensing performance of TiO_2 nanofilms by automated nebulizer spray pyrolysis technique," *Optik (Stuttg).*, vol. 127, no. 23, pp. 11102–11110, 2016.

[14] H. Masoumi, R. Haghighi, and S. M. Mirfendereski, "Thermochimica Acta Modification of physical and thermal characteristics of stearic acid as a phase change materials using TiO_2 -nanoparticles," *Thermochim. Acta*, vol. 675, no. December 2018, pp. 9–17, 2019.

[15] S. Shen *et al.*, "Titanium dioxide nanostructures for photoelectrochemical applications," *Prog. Mater. Sci.*, vol. 98, no. October 2017, pp. 299–385, 2018.

[16] G. Kaur, P. Negi, M. Kaur, R. Sharma, R. J. Konwar, and A. Mahajan, "Morpho-structural and opto-electrical properties of chemically tuned nanostructured TiO_2," *Ceram. Int.*, vol. 44, no. 15, pp. 18484–18490, 2018.